Regulation of FMRP granule structure and function through phosphorylation

Shivani C. Kharod[1], Dongwoo Hwang[2], Pablo E. Castillo[1,3] and Young J. Yoon[1,2,*]

[1] Dominick P. Purpura Department of Neuroscience, Albert Einstein College of Medicine, NY 10461
[2] Department of Cell Biology, Albert Einstein College of Medicine, NY 10461
[3] Department of Psychiatry and Behavioral Sciences, Albert Einstein College of Medicine, NY 10461

Running title: Regulation of FMRP granule structure and function through phosphorylation

* Correspondence:

Young J. Yoon, Ph.D.
Dominick P. Purpura Department of Neuroscience
Albert Einstein College of Medicine
1300 Morris Park Avenue
Bronx, NY 10461
USA
Email: young.yoon@einsteinmed.edu

Abstract

Fragile X messenger ribonucleoprotein (FMRP) is an RNA-binding protein that can form granules within neurons. Although FMRP-containing Fragile X granules have been extensively characterized, visualizing changes in granule structure in relation to function has been difficult. We used high-resolution imaging to detect discrete differences in puncta size, intensity, and contrast in our mouse FMRP and serine 499 (S499) phospho-mutant reporters. Tracking analyses of FMRP particles showed that phospho-mutant granules traveled at rates consistent with active transport within dendrites. In addition, GFP-FMRP exhibited a wide range of speeds owing to its ability to oligomerize when overexpressed. Recent work suggested that FMRP granules could be phase separated structures that may function as hubs for local protein synthesis. To test this idea, we performed fluorescence recovery after photobleaching (FRAP) on individual FMRP granules. Intriguingly, we observed only a partial recovery that occurred over minutes and was dependent on translation. Moreover, the phospho-mutants displayed differences in recovery kinetics reflecting the labile (S499A) or preferential (S499D) nature of their interaction with granules containing stalled ribosomes. Our high-resolution approach reveals that the phosphorylation-state of FMRP can modulate the clustering of FMRP granules and thereby regulate local protein synthesis at the level of individual granules.

Introduction

Fragile X messenger ribonucleoprotein (FMRP) is an RNA-binding protein with roles in mRNA transport and protein synthesis[1-3], where the loss of expression can lead to intellectual disability with links to autism[4]. In *Fmr1* knock-out mice, the absence of FMRP led to elevated protein production and altered synaptic plasticity[5,6]. At the molecular level, studies have shown that FMRP interacts with translating polyribosomes[7,8] and mRNA[9,10] to regulate protein synthesis and travel along dendrites in an activity-dependent manner[11,12]. In addition, recent studies have elucidated different mechanisms of translational repression by FMRP through interactions with various translation components, such as the FMRP-interacting factor, CYFIP1[13], stalled ribosomes[10] and microRNA complexes[14]. Although it is unclear whether all three modes of translation inhibition co-occur simultaneously on FMRP target mRNAs, it is clear that FMRP plays a central role in regulating local protein synthesis.

One prominent feature of FMRP in neurons is the formation of granules[12,15-17]. FMRP is a multivalent protein with the ability to interact with mRNA, ribosomes, as well as other regulatory proteins for transport and translational control in dendrites[2,18]. FMRP can also bind with itself to mediate self-assembly into these relatively large intracellular structures[19,20]. Known as Fragile X granules (FXG), FMRP-containing granules are also abundantly present in axons[17,21]. Expression of fluorescent FMRP can readily detect these punctate structures that coincide with mRNA and move bidirectionally along dendrites and axons[11,22]. However, visualization of FMRP dynamics has been challenging due to its abundant nature and ability to move along dendrites.

Phosphorylation of FMRP was first identified in flies, where it was shown to be necessary for RNA-binding and homomer formation in vitro[23]. In mice, FMRP phosphorylation on serine 499 (S499) was found to not affect its interaction with RNA, but rather its association with polyribosomes and provided early indications that phosphorylated FMRP preferentially bound stalled ribosomes[24]. Subsequently, it was shown that activation of metabotropic glutamate receptors (mGluR) led to brief dephosphorylation of FMRP by protein phosphatase 2A (PP2A)[25] and facilitated the local translation of *Arc* in dendrites[26]. Dephosphorylation of FMRP by PP2A also led to rapid degradation of FMRP by the proteasome[27]. Taken together, these studies point to phosphorylation of S499 as a critical determinant in regulating protein synthesis.

While there is compelling evidence that FMRP granules can undergo rapid activity-dependent trafficking and remodeling to facilitate protein synthesis[25,26], what is less understood is how FMRP function relates

to granule structure. Numerous models have been proposed where FMRP granules dissolve and release mRNA for translation to occur, but evidence to support such models have been indirect. Whether granule disassembly was necessary and sufficient for local protein synthesis has been difficult to demonstrate without direct observation. Recently, a new hypothesis was proposed to bridge this gap via the identification of a low complexity region (LCR) on FMRP that encompasses the unstructured C-terminus of FMRP, including the RGG box[28,29]. There is emerging evidence that RNA-protein complexes can form condensates or membraneless compartments through phase separation[30]. Previously, mRNAs and polysomes have been classified as transport granules or neuronal RNA granules, but the mechanism by which these structures facilitated local protein synthesis was incomplete[31,32]. Hence, the idea that FMRP granules could utilize phosphorylation in order to attract and enrich components of translation through phase separation remains highly suggestive.

Here, we use fluorescent reporters of FMRP and S499 phospho-mutants (S499A and S499D) to detect changes in their granule dynamics. Our results show that each reporter exhibits differences in granule properties that are consistent with their ability to interact with FMRP granules. Moreover, fluorescence recovery after photobleaching (FRAP) on individual FMRP granules revealed slow recovery kinetics that differed depending on their preference for polysome-binding. Thus, our results demonstrate that a high-resolution approach can be an effective way to determine how individual granule dynamics mediates local protein synthesis.

Results

Fluorescent FMRP reporters form discrete granules in neurons

To better understand the relationship between FMRP granule structure and function, we first generated a lentiviral expression construct of GFP-tagged FMRP (GFP-FMRP)[24] under the control of the human Synapsin promoter to limit expression to neurons (Fig. 1a). GFP-FMRP has previously been shown to assemble into granules[12,33] and we performed immunofluorescence using antibodies to FMRP (Abcam) and GFP (Aves lab) to confirm that GFP-FMRP colocalized with endogenous FMRP in dendrites (Fig. S1a). We also co-expressed GFP-FMRP with Halo-FMRP[34] to demonstrate that FMRP with different tags could associate with each other in granules (Fig. S1b). When we co-express GFP-FMRP with ribosomal protein L10A fused to HaloTag, we observed colocalization of granules with ribosomes (Fig. S1c). Although neurons are sensitive to overexpression of FMRP[35], we expressed our FMRP reporters in wildtype mouse neurons to minimize the potential perturbation of endogenous FMRP granule formation during development in culture, with the broader goal of visualizing differences in FMRP granules. Next, we prepared the phosphodeficient (S499A) and phosphomimetic (S499D) FMRP reporters[24] to ask whether the phosphorylation state of FMRP on S499 could alter granule dynamics. To determine the optimal expression level for granule visualization in dendrites, we infected cultured hippocampal neurons with our reporters for one-week (Fig. 1b,c). When we attempted a shorter 3-day expression (Fig. S1d), the reporters exhibited very little quantifiable differences in dendrites (Fig. S1e-g) likely due to insufficient levels of expression to visualize changes in granules. Conversely, longer expression (> 10 days) typically led to overlapping puncta in dendrites where individual granules could not be optically resolved. Optimizing the levels of reporter expression was important to limit overexpression to a range that would yield quantitative differences from fluorescence imaging and particle analysis by TrackMate[36] in FIJI (ImageJ) (Fig. 1d,e).

FMRP and S499 phospho-mutant reporters form distinct granules

To characterize the FMRP granules formed by our reporters, we quantified the puncta size, fluorescence intensity and particle contrast for each neuron imaged and plotted their average values (Fig. 1f-h). We also included quantification of β-actin mRNA, which has been previously characterized[37,38], to serve as a control for particle detection. The median size of GFP-FMRP puncta was around 0.5 μm, which was consistent with previous reports[16]. The S499A mutant formed smaller granules on average (Fig. S2a) and conversely S499D mutant formed slightly larger granules (Fig. S2b), relative to GFP-FMRP, supporting the observation that the charge from the added phosphate groups could facilitate assembly of FMRP into

larger granules. What was more striking was the differences in intensities among the various reporters. In comparison to the 3-day expression (Fig. S1f), GFP-FMRP showed a relatively large shift in distribution of average puncta intensity, while S499A remained unchanged and S499D puncta intensity showed a slight increase. These differences in puncta intensity between GFP-FMRP and the phospho-mutants suggested that cycles of phosphorylation and dephosphorylation were necessary for smaller FMRP granules to form larger granules and promote homotypic interactions under overexpression conditions. Intriguingly, the S499D mutant which was expected to mimic phosphorylated FMRP, did not exhibit bright granules on average. Although we detected high-intensity S499D granules, we also observed a large population of low-intensity puncta that may have lowered the overall average value (Fig S2b). As it had been reported that S499D mutant preferentially binds to stalled polyribosomes[24], perhaps they can also interact with stalled monosomes that do not coalesce into large granules resulting in the observation of smaller puncta. Next, we wanted to analyze the granularity of FMRP particles by comparing puncta contrast. Contrast is typically defined as the difference between the intensity inside and outside of the puncta and can be a measure of how clustered a fluorescent granule is formed[39]. Thus, particle contrast values can indicate whether the FMRP reporter was tightly or loosely bound to a granule and points to how well each reporter can cluster. Notably, we observed a bimodal clustering distribution from the mutants, where S499A had higher and S499D had lower contrast values relative to the GFP-FMRP reporter. Taken together, our results suggest that S499A forms granules that are smaller and more compact while the S499D forms granules that are larger and diffuse granules.

FMRP promotes granule multimerization

Comparison of fluorescent FMRP puncta intensities between GFP-FMRP and the phospho-mutants shows that GFP-FMRP granules can exhibit more than 2-fold higher intensity (Fig. 1g). Although this may be a consequence of overexpression, we wanted to explore the ability of GFP-FMRP reporter to multimerize through the association with other FMRP granules. When we initially compared the population of granule sizes from a single cell, we observed an interesting difference where the S499A mutant was not able to form larger fluorescent puncta compared to GFP-FMRP (Fig. S3a). In the violin plot, GFP-FMRP formed three discrete populations where the radius appeared to approximately double (1x, 2x, 4x), while the S499A mutant had only a major population of the smallest granules along with trace amounts of the larger particles. Such step-wise increase in puncta size, opposed to a gradual increase, supports the idea that FMRP granule multimerization requires S499 phosphorylation to facilitate formation of higher-order structures of FMRP granules. We extended this analysis to include every FMRP puncta and show that while

the median population was similar for all reporters, the upper and lower quartile populations varied between the phospho-mutants indicating a shift in granule size (Fig. S3b). Also the three major populations in the aggregate plots persist, further suggesting that multimerization is a feature of FMRP granules. The stacked bar graph represents the various granule sizes as a fraction of the entire population (Fig. S3c).

FMRP reporters differ in processive movement

FMRP granules travel throughout neurons[11,22,33]. One difficulty in tracking actively-transported molecules or complexes in dendrites is the timescale at which motion can be observed and studied. Previously, we have shown that endogenous β-actin mRNA can burst into movement along dendrites for several seconds followed by long pauses which can last for minutes[38]. Moreover, as we cannot anticipate whether a particular granule or mRNA would move, post hoc analyses of movies are required to extrapolate their motion. We acquired short continuous streaming images (50 ms per frame for 1000 frames) of randomly-selected neurons expressing the FMRP reporter (Fig. S4). Next, we used Image J plugin TrackMate (LAP tracker) to perform tracking of all moving and non-moving particles (Fig. 2a). Previous studies had reported that FMRP granules typically appear static and immobile in dendrites and our tracking analyses also confirmed that only around 12% or less of identified tracks moved in excess of 0.5 μm from their original position during our imaging epoch (Fig. 2b). However, to gain further insight into FMRP particles that are engaged in processive movement, we chose to focus our analysis on trajectories with large displacements (> 1.5 μm). While such a stringent criteria led to a small proportion of tracks (~0.1%), differences began to emerge between these populations. When we plotted the average speed of each processive FMRP puncta, we observed that GFP-FMRP granules had a wide distribution of average velocities ranging from 0.2-8.0 μm/sec with a median of around 4 μm/sec. A majority of these granules were traveling faster than those reported for individual mRNA molecules in dendrites which typically transit at 2 μm/sec (Fig. 2c)[37]. The phospho-mutant granules were noticeably slower compared to GFP-FMRP but closer to β-actin mRNA. These observations are consistent with GFP-FMRP granules multimerizing which can lead to recruitment of a larger number of motor proteins, which S499A or S499D could not achieve. Notably, the S499D phosphomimic mutant exhibited the slowest speeds among the FMRP reporters, suggesting that while S499D can move, they tended to impede FMRP granule trafficking in dendrites. However, observation of a slow (< 2 μm/sec) and a fast (> 2 μm/sec) population within the S499D distribution led us to ask whether size of these high displacing granules could affect the speed. When we looked at the sizes of the granules that traveled processively, GFP-FMRP was significantly larger

than S499A with a median diameter of 0.6 μm while S499A granules were similar to their population average (Fig. 2d). Next, to address whether there was a correlation we plotted the speed and the size of each moving FMRP granule (Fig. 2e-h). The GFP-FMRP granules exhibited a positive correlation between size and speed (R^2 = 0.49), where larger particles traveled faster. While a majority of the S499A particles had a positive correlation between speed and size (R^2 = 0.47), the granules did not exhibit higher speed or size in comparison to GFP-FMRP. The S499D granules were much less correlated where size of the granule was not an indicator of speed (R^2 = 0.23). We also included the plot of β-actin mRNA, which showed poor correlation between size and speed, as expected (R2 = 0.10). These results demonstrate that larger GFP-FMRP granules can engage in processive movement as a consequence of multimerization, while the phospho-mutants are restricted in their transport due to either being unable to multimerize (S499A) or due to inefficiently interaction with motor proteins.

FMRP granules resemble gel-like structures

The identification of the C-terminal portion of FMRP as a low-complexity region (LCR) was intriguing as it hinted that the granular structure of FMRP had functional consequences[28]. As FMRP has multiple RNA-binding domains that associate with mRNA such as the KH1 domain and RGG-box, along with the ability to bind ribosomes through the KH2 domain, it was suggestive that FMRP may undergo liquid-liquid phase separation (LLPS) as it formed granules[40]. One criteria of LLPS is that components can freely exchange with the other phase. As such, fluorescence recovery after photobleaching (FRAP) assay can readily validate phase separation, where fast recovery kinetics (within several seconds) serve as confirmation of rapid subunit exchange. We set out to perform FRAP on individual fluorescent granules of average size to test whether FMRP molecules within the granule would freely exchange with other FMRP molecules nearby. We used a brief pulse of focused UV-light to target a single GFP-FMRP fluorescent puncta and to minimize UV exposure to the remaining dendrite within the field of view (Fig. 3a). It became apparent that fluorescence recovery on FMRP granules was a slow process where we did not detect a robust recovery within 1-2 minutes. We opted to acquire longer time-lapse images (20 mins) to determine whether recovery could be observed (Fig. 3b,c). We also performed our FRAP assay at two different temperatures (22 ^{o}C and 35 ^{o}C), to see how temperature affected recovery of FMRP molecules in granules. Our FRAP results indicated that GFP-FMRP granules recovered slightly faster at 35 ^{o}C and reaching around 40% recovery after 20 minutes (τ = 147.3 s), while at 22 ^{o}C we only observed a 30% recovery (τ = 172.5 s) (Fig. 3d,g). We observed similar recovery kinetics with S499A, with 40% recovery at both temperatures tested (Fig. 3e,h), suggesting that S499A recovery was insensitive to temperature in its association with the

granule. In contrast, S499D recovered very slowly (τ = 256.5 s) at 22 ^{o}C. Surprisingly, S499D recovered very little at 35 ^{o}C (τ = 64.4 s), with only a 10% recovery on average after taking into account the bleaching efficiency (Fig. 3f,i). Overall, the rates of recovery were inconsistent with LLPS and indicated a timescale of hours for full recovery. While there is much interest in phase separation, there is growing understanding that perhaps intracellular droplets under certain situations can transition into liquid-gel state[41]. To test this idea, we generated reporters with a light-induced oligomerization domain, CRY2olig[42], fused to FMRP, with the intent to use light to promote clustering of FMRP. When we expressed these constructs in neurons, the granules were very static and did not respond to light-induction. Also the granules were very bright, while retaining granule size and contrast values similar to GFP-fusion reporters (Fig. S5). Through the addition of an oligomerization domain (CRY2) onto FMRP, the homomeric affinity of FMRP was enhanced and pushed the granules into supersaturated solid-like gels[41]. Although we cannot conclude that we observe LLPS in FMRP granules, perhaps there could be a core of FMRP-interactors that may facilitate phase separation in an activity-dependent manner.

FMRP granules undergo translation

In addition to the slow recovery kinetics, the recovery plateaus after 10 minutes under all conditions. As we were spot-bleaching the granule, it was unlikely that FMRP molecules were rate-limiting in the recovery, but rather that the granule had reached a steady-state equilibrium between inside and outside of the granule where it was undergoing exchange at a minutes timescale. One possible explanation was protein synthesis, a process which FMRP has been linked to through its association with the ribosome. To test this idea, we performed FRAP in the presence of a translation elongation inhibitor, cycloheximide (CHX) which would result in stalled ribosomes (Fig. 4a). In addition, our FRAP assay was performed at 22 ^{o}C to minimize unanticipated events of particles passing through or transiently docking near the site of the photobleached puncta. Interestingly, GFP-FMRP granules failed to recover in the presence of CHX (Fig. 4b, brown), suggesting that FMRP bound to stalled ribosomes do not exchange with unbound FMRP. The S499A mutant initially recovers at a rate similar to FRAP at 22 ^{o}C and then gradually decreases (Fig. 4c), suggesting that interaction of S499A with stalled ribosomes was quite labile. On the other hand, the S499D mutant can be observed rapidly recovering under CHX-treatment (Fig. 4d), confirming that phosphorylated FMRP preferentially binds to stalled ribosomes and recovers to levels similar to FRAP without CHX. To understand the observed decrease in recovery in FRAP with CHX, we generated bleach curves for our FRAP assay and found that CHX-treatment generally led to a 10-20% loss in fluorescence

signal at the end of the imaging (Fig. S6) which can explain the negative slopes of the recovery curves. One explanation for this reduction could be that by stalling ribosomes and locking FMRP onto granules by CHX, the static granules became more photolabile and also reduced the free population of FMRP that could exchange with the photobleached FMRP. In sum, our results suggest that FMRP granules are capable of protein synthesis and that the phosphorylation state of FMRP can modulate the affinity of FMRP for translating or stalled ribosomes in order to provide spatiotemporal control over local protein synthesis.

Discussion

In this study, we examined how FMRP phosphorylation can regulate granule function through the use of fluorescent reporters and high resolution microscopy. FMRP phosphorylation on S499 acts, not only as a molecular switch, but also as a key structural determinant of granule formation (Fig. 1), multimerization (Fig. S3), transport (Fig. 2) and translation (Figs. 3,4). By visualizing how phospho-mutant granules differ from GFP-FMRP granules, we can begin to appreciate the structure of FMRP granules in relation to function. It is also important to acknowledge that phosphorylation is a dynamic process where FMRP exists in an equilibrium of phosphorylated and unphosphorylated states in order to function properly[25,27]. As such, our reporters can be useful tools to investigate FMRP function and dysfunction.

An important but overlooked feature of FMRP is its ability to self-assemble. While it was first identified in 2003, these structures were overlooked as aggregates of overexpression. Now, as we understand more about RNA-protein interactions, we are discovering that certain protein domains can have intrinsic properties to self-assemble[30]. Despite numerous biochemical studies showing that components of translation were abundantly present in neuronal RNA granules[31,32], without the ability to look at individual granules dynamically in living cells it was difficult to conclude that these were biologically relevant structures. Nevertheless, many localized RNAs are transported as ribonucleoprotein (RNP) complexes often bound to ribosomes which can provide the necessary seeding density or molecular crowding for phase separation[43]. Our results indicate that homomeric interaction is a necessary feature of FMRP granule formation and multimerization. Although our results are not fully consistent with LLPS, the idea that the FMRP LCR serves to potentially mediate recruitment of granule related CAPRIN1[29] or FUS[44] provides an alternative explanation to an unresolved question.

The highest level of recovery observed in our FRAP assay was around 40% (Fig. 3). Although we have shown that the recovery was translation-dependent, there is a larger population of FMRP that does not recover and is translation-independent. The likely source of this unrecoverable FMRP is bound at the untranslated regions (UTRs) of mRNA. There are differing opinions on whether FMRP can bind RNA in a sequence-specific manner[10,45] and our results may be consistent with both interactions with the ribosomes and the UTRs. Moreover, if FMRP bound to CYFIP1[13] or microRNA complexes[14] are also present, it is not impossible to imagine a significant population of FMRP that is not ribosome-associated.

One surprising result from this study was that FMRP granules were engaged in translation. As FMRP has been shown to be a negative regulator of translation, the results seemed to contradict consensus view. Although FMRP function has been simplified to all-or-none outcomes in many instances, it is likely that FMRP functions somewhere in between working in conjunction with other available factors to regulate protein synthesis, such as mRNA stability through codon optimality[46], nonsense-mediated decay (NMD)[47] or m6A-mediated decay[48], all of which may not directly lead to stalling ribosomes. Moreover, it will be necessary to characterize the translation rate of non-FMRP target mRNAs to ascertain whether what we are observing is already a consequence of reduced translation rates by FMRP.

Methods

Animal work was performed in accordance with Institutional Animal Care and Use Committee protocols at Albert Einstein College of Medicine. Plasmids used in this work are available on Addgene. Detailed protocols and reagent information herein are available upon request.

Plasmids and lentivirus production

Lentiviral expression vectors for GFP-FMRP, GFP-FMRP S499A and GFP-FMRP S499D were prepared by restriction digest cloning using PCR amplification of EGFP-FMRP sequence from p-EGFP-C1-Flag-mFmr1(wt), p-EGFP-C1-Flag-mFmr1(A) and p-EGFP-C1-Flag-mFmr1(D), respectively. The EGFP-FMRP plasmids were a gift from Stephanie Ceman (Addgene plasmids #87929, #87913 and #87914). Lentiviral particles were generated by transfecting ENV (pMD2.VSVG), packaging (pMDLg/pRRE), REV (pRSV-Rev) along with the expression vector into HEK293T cells using calcium phosphate transfection. Viral supernatant was concentrated using Lenti-X concentrator (Takara Bio) according to manufacturer's instruction. Virus was resuspended in Neurobasal A (Invitrogen) and stored at -80 ^{o}C.

Dissociated mouse hippocampal neuron culture

Post-natal day 1 (P1) mouse hippocampal tissue was isolated from C57BL/6 wildtype newborn pups. Hippocampi were dissociated in 0.25% trypsin, triturated and plated onto poly-D-lysine (Sigma) coated glass-bottomed dishes (MatTek) at 35,000-50,000 cells per dish. Neurons were cultured in Neurobasal A supplemented with B-27 (Invitrogen) and GlutaMAX (Invitrogen).

Sample preparation and imaging

Cultured hippocampal neurons were infected with lentivirus at DIV7 and imaged after one week at DIV14, unless noted otherwise. Prior to imaging, the media was exchanged to Hiberate A low fluorescence (BrainBits) and allowed to equilibrate for 30 minutes prior to imaging at 22 ^{o}C or 35 ^{o}C. For FMRP reporter particle detection and tracking, we acquired continuous images at 50 ms per frame for 1000 frames at a single plane. For the FRAP assay, we acquired time-lapse z-series (21 steps at 0.2 μm per step) at 30 second intervals for 40 time-points. For HaloTag labeling, cells were treated with 10 nM JF549HTL or JF646HTL for 15 minutes, followed by 3x washes and incubation in Hibernate A for at least one hour. Cells were washed again prior to imaging. For immunofluorescence, neuron were fixed in 4% paraformaldehyde solution and permeabilized. After blocking in normal goat serum, cells were treated with primary antibodies: anti-GFP (Aves lab) or anti-FMRP (Abcam; ab17722), followed by secondary antibodies: Goat

anti-chicken Alexa Fluor 647 (Thermo Fisher) or goat anti-rabbit Cy3 (Sigma) and DAPI. Images were 512x512 in size with a pixel size of 106.7 nm. All z-series images were maximum projected prior to analysis.

Fluorescence microscopy

Acquisition of fluorescence images were performed on a wide field microscope previously described[38]. In brief, the inverted wide field microscope was equipped with 491 nm (Cobolt), 561 nm (Lasertechnik) and 640 nm (Coherent) laser lines along with a 150x 1.45 NA oil immersion objective (Olympus). Images were acquired on an EMCCD camera (Andor). For photobleaching FMRP puncta, we used a 405 nm UV laser (Omikron) along with a motorized focus lens (Thorlabs). The cells were maintained at 35 ^{o}C throughout imaging through a humidified stage top incubator (Tokai Hit).

Image analysis

Analyses of all imaging data were performed using FIJI (ImageJ). For particle detection and tracking we used the ImageJ plugin TrackMate[36]. We used the Laplacian of Gaussian filter for detection where the *estimated blob diameter* was set to 5 pixels and *threshold* at 30. These values were determined empirically by evaluating several randomly selected reference images of GFP-FMRP and determining the contrast of all particles detected. Under those conditions, we are able to filter out puncta with negative contrast values. We also selected to use *median filter* and *sub-pixel localization* for better gaussian fit of fluorescent puncta. These conditions were applied identically to all images to maintain consistency in the analysis. For tracking, we used the default settings for Simple LAP tracker with *maximum linking distance* of 15 pixels and *maximum gap-closing distance* of 15 pixels. The *maximum gap-closing frame gap* was set to 2. Kymographs of trafficking puncta were generated using the ImageJ plugin Kymographbuilder. For FRAP analysis, we selected a 9-pixel circle as the bleach puncta ROI and measured average pixel intensity within the ROI for all time-point. The average intensity values were normalized to pre image (t = -30 sec) and the error bars denote standard deviation. The fluorescence recovery values were fit to a nonlinear regression curve to derive time constants (τ) of the recovery. The bleach curves for the FRAP assay were calculated by measuring average intensity in a region (9-pixel ROI) that was not photobleached and normalized to pre image (t = -30 sec).

Figure legends

Fig. 1 ***Fluorescent FMRP reporters form discrete puncta in neurons*****.** **a** Schematic of FMRP reporter constructs: GFP-FMRP, S499A and S499D mutants. **b** Timeline of experiment. **c** A 10x magnification view of cultured neurons expressing GFP-FMRP labeled with antibodies to GFP. Scale bar is 50 μm. **d** A representative dendrite expressing GFP-FMRP (top panel, inverted grayscale). Dendrite represented in 16-color LUT (middle panel). Dendrite overlaid with TrackMate puncta detection (bottom panel). Scale bar is 5 μm. **e** Surface plot of puncta shown in the dotted box in **d**. Violin plots of puncta diameter (**f**), intensity (**g**) and contrast (**h**) from neurons expressing FMRP reporters: GFP-FMRP (green), S499A (magenta), S499D (blue) and β-actin mRNA (gray). GFP-FMRP (n=32), S499A (n=36), S499D (n=14) and β-actin mRNA (n=15). Statistical significance was calculated using unpaired, two-tailed student's t-test. p** < 0.01; p**** < 0.0001.

Fig. 2 ***FMRP reporters differ in processive movement.*** **a** Fluorescence images of GFP-FMRP (top), S499A (middle) and S499D (bottom) expressing dendrites overlaid with tracks detected by TrackMate. LUT indicates velocity at μm/sec and the scale bar is 5 μm. **b** Stacked bar graph showing the fraction of trajectories that traveled less than 0.5 μm (red bars) or greater than 0.5 μm (green bars) for each reporter and β-actin mRNA. To identify the most processive particles, we selected granules that displaced greater than 1.5 μm and plotted their velocity (**c**) and size (**d**). Scatter plots of granule size vs velocity overlaid with linear regression fit for (**e**) GFP-FMRP (green; 112 out of 83,954 tracks), (**f**) S499A (magenta; 134 out of 45,991 tracks), (**g**) S499D (blue; 40 out of 30,242 tracks) and (**h**) β-actin mRNA (gray; 33 out of 2,742).

Fig. 3 ***FMRP granules are slow to exchange FMRP proteins.*** **a** Schematic of our spot photobleaching of individual FMRP granules. **b** Representative GFP-FMRP granule FRAP assay. The white arrow indicates the granule to be photobleached and the scale bar is 2 μm. **c** Time-series montage of FMRP granule FRAP. Time is noted on the top-right in seconds. Plot of average fluorescence recovery ± SD for GFP-FMRP at 22 °C (**d**) and at 35 °C (**g**), S499A at 22 °C (**e**) and at 35 °C (**h**) and S499D at 22 °C (**f**) and at 35 °C (**i**). The recovery values were fit to a nonlinear regression curve to derive time constants (τ) of recovery.
GFP-FMRP at 22 °C (n = 12), at 35 °C (n = 13); S499A at 22 °C (n = 10), at 35 °C (n = 10); S499D at 22 °C (n = 12), at 35 °C (n = 13);

Fig. 4 ***FMRP granules under go protein synthesis.*** **a** Schematic of the FRAP assay in the presence of cycloheximide (CHX). **b** Plot of GFP-FMRP FRAP at 22 °C with (brown) or without (blue) CHX. **c** Plot of S499A FRAP at 22 °C with (brown) or without (blue) CHX. **d** Plot of S499D FRAP at 22 °C with (brown) or without (blue) CHX.

References

1 Bagni, C. & Zukin, R. S. A Synaptic Perspective of Fragile X Syndrome and Autism Spectrum Disorders. *Neuron* **101**, 1070-1088, doi:10.1016/j.neuron.2019.02.041 (2019).

2 Richter, J. D., Bassell, G. J. & Klann, E. Dysregulation and restoration of translational homeostasis in fragile X syndrome. *Nat Rev Neurosci* **16**, 595-605, doi:10.1038/nrn4001 (2015).

3 Darnell, J. C. & Klann, E. The translation of translational control by FMRP: therapeutic targets for FXS. *Nat Neurosci* **16**, 1530-1536, doi:10.1038/nn.3379 (2013).

4 Hagerman, R. J. *et al.* Fragile X syndrome. *Nat Rev Dis Primers* **3**, 17065, doi:10.1038/nrdp.2017.65 (2017).

5 Qin, M., Kang, J., Burlin, T. V., Jiang, C. & Smith, C. B. Postadolescent changes in regional cerebral protein synthesis: an in vivo study in the FMR1 null mouse. *J Neurosci* **25**, 5087-5095, doi:10.1523/JNEUROSCI.0093-05.2005 (2005).

6 Huber, K. M., Gallagher, S. M., Warren, S. T. & Bear, M. F. Altered synaptic plasticity in a mouse model of fragile X mental retardation. *Proc Natl Acad Sci U S A* **99**, 7746-7750, doi:10.1073/pnas.122205699 (2002).

7 Stefani, G., Fraser, C. E., Darnell, J. C. & Darnell, R. B. Fragile X mental retardation protein is associated with translating polyribosomes in neuronal cells. *J Neurosci* **24**, 7272-7276, doi:10.1523/JNEUROSCI.2306-04.2004 (2004).

8 Khandjian, E. W. *et al.* Biochemical evidence for the association of fragile X mental retardation protein with brain polyribosomal ribonucleoparticles. *Proc Natl Acad Sci U S A* **101**, 13357-13362, doi:10.1073/pnas.0405398101 (2004).

9 Brown, V. *et al.* Microarray identification of FMRP-associated brain mRNAs and altered mRNA translational profiles in fragile X syndrome. *Cell* **107**, 477-487, doi:10.1016/s0092-8674(01)00568-2 (2001).

10 Darnell, J. C. *et al.* FMRP stalls ribosomal translocation on mRNAs linked to synaptic function and autism. *Cell* **146**, 247-261, doi:10.1016/j.cell.2011.06.013 (2011).

11 Antar, L. N., Afroz, R., Dictenberg, J. B., Carroll, R. C. & Bassell, G. J. Metabotropic glutamate receptor activation regulates fragile x mental retardation protein and FMR1 mRNA localization differentially in dendrites and at synapses. *J Neurosci* **24**, 2648-2655, doi:10.1523/JNEUROSCI.0099-04.2004 (2004).

12 Dictenberg, J. B., Swanger, S. A., Antar, L. N., Singer, R. H. & Bassell, G. J. A direct role for FMRP in activity-dependent dendritic mRNA transport links filopodial-spine morphogenesis to fragile X syndrome. *Dev Cell* **14**, 926-939, doi:10.1016/j.devcel.2008.04.003 (2008).

13 Napoli, I. *et al.* The fragile X syndrome protein represses activity-dependent translation through CYFIP1, a new 4E-BP. *Cell* **134**, 1042-1054, doi:10.1016/j.cell.2008.07.031 (2008).

14 Muddashetty, R. S. *et al.* Reversible inhibition of PSD-95 mRNA translation by miR-125a, FMRP phosphorylation, and mGluR signaling. *Mol Cell* **42**, 673-688, doi:10.1016/j.molcel.2011.05.006 (2011).

15 Estes, P. S., O'Shea, M., Clasen, S. & Zarnescu, D. C. Fragile X protein controls the efficacy of mRNA transport in Drosophila neurons. *Mol Cell Neurosci* **39**, 170-179, doi:10.1016/j.mcn.2008.06.012 (2008).
16 El Fatimy, R. *et al.* Tracking the Fragile X Mental Retardation Protein in a Highly Ordered Neuronal RiboNucleoParticles Population: A Link between Stalled Polyribosomes and RNA Granules. *PLoS Genet* **12**, e1006192, doi:10.1371/journal.pgen.1006192 (2016).
17 Christie, S. B., Akins, M. R., Schwob, J. E. & Fallon, J. R. The FXG: a presynaptic fragile X granule expressed in a subset of developing brain circuits. *J Neurosci* **29**, 1514-1524, doi:10.1523/JNEUROSCI.3937-08.2009 (2009).
18 Lai, A., Valdez-Sinon, A. N. & Bassell, G. J. Regulation of RNA granules by FMRP and implications for neurological diseases. *Traffic* **21**, 454-462, doi:10.1111/tra.12733 (2020).
19 Adinolfi, S. *et al.* The N-terminus of the fragile X mental retardation protein contains a novel domain involved in dimerization and RNA binding. *Biochemistry* **42**, 10437-10444, doi:10.1021/bi034909g (2003).
20 Zhang, Y. *et al.* The fragile X mental retardation syndrome protein interacts with novel homologs FXR1 and FXR2. *EMBO J* **14**, 5358-5366, doi:10.1002/j.1460-2075.1995.tb00220.x (1995).
21 Akins, M. R. *et al.* Axonal ribosomes and mRNAs associate with fragile X granules in adult rodent and human brains. *Hum Mol Genet* **26**, 192-209, doi:10.1093/hmg/ddw381 (2017).
22 Antar, L. N., Li, C., Zhang, H., Carroll, R. C. & Bassell, G. J. Local functions for FMRP in axon growth cone motility and activity-dependent regulation of filopodia and spine synapses. *Mol Cell Neurosci* **32**, 37-48, doi:10.1016/j.mcn.2006.02.001 (2006).
23 Siomi, M. C., Higashijima, K., Ishizuka, A. & Siomi, H. Casein kinase II phosphorylates the fragile X mental retardation protein and modulates its biological properties. *Mol Cell Biol* **22**, 8438-8447, doi:10.1128/MCB.22.24.8438-8447.2002 (2002).
24 Ceman, S. *et al.* Phosphorylation influences the translation state of FMRP-associated polyribosomes. *Hum Mol Genet* **12**, 3295-3305, doi:10.1093/hmg/ddg350 (2003).
25 Narayanan, U. *et al.* FMRP phosphorylation reveals an immediate-early signaling pathway triggered by group I mGluR and mediated by PP2A. *J Neurosci* **27**, 14349-14357, doi:10.1523/JNEUROSCI.2969-07.2007 (2007).
26 Niere, F., Wilkerson, J. R. & Huber, K. M. Evidence for a fragile X mental retardation protein-mediated translational switch in metabotropic glutamate receptor-triggered Arc translation and long-term depression. *J Neurosci* **32**, 5924-5936, doi:10.1523/JNEUROSCI.4650-11.2012 (2012).
27 Nalavadi, V. C., Muddashetty, R. S., Gross, C. & Bassell, G. J. Dephosphorylation-induced ubiquitination and degradation of FMRP in dendrites: a role in immediate early mGluR-stimulated translation. *J Neurosci* **32**, 2582-2587, doi:10.1523/JNEUROSCI.5057-11.2012 (2012).
28 Tsang, B. *et al.* Phosphoregulated FMRP phase separation models activity-dependent translation through bidirectional control of mRNA granule formation. *Proc Natl Acad Sci U S A* **116**, 4218-4227, doi:10.1073/pnas.1814385116 (2019).

29 Kim, T. H. *et al.* Phospho-dependent phase separation of FMRP and CAPRIN1 recapitulates regulation of translation and deadenylation. *Science* **365**, 825-829, doi:10.1126/science.aax4240 (2019).
30 Chen, X., Wu, X., Wu, H. & Zhang, M. Phase separation at the synapse. *Nat Neurosci* **23**, 301-310, doi:10.1038/s41593-019-0579-9 (2020).
31 Kanai, Y., Dohmae, N. & Hirokawa, N. Kinesin transports RNA: isolation and characterization of an RNA-transporting granule. *Neuron* **43**, 513-525, doi:10.1016/j.neuron.2004.07.022 (2004).
32 Krichevsky, A. M. & Kosik, K. S. Neuronal RNA granules: a link between RNA localization and stimulation-dependent translation. *Neuron* **32**, 683-696, doi:10.1016/s0896-6273(01)00508-6 (2001).
33 Antar, L. N., Dictenberg, J. B., Plociniak, M., Afroz, R. & Bassell, G. J. Localization of FMRP-associated mRNA granules and requirement of microtubules for activity-dependent trafficking in hippocampal neurons. *Genes Brain Behav* **4**, 350-359, doi:10.1111/j.1601-183X.2005.00128.x (2005).
34 Monday, H. R., Kharod, S. C., Yoon, Y. J., Singer, R. H. & Castillo, P. E. Presynaptic FMRP and local protein synthesis support structural and functional plasticity of glutamatergic axon terminals. *Neuron* **110**, 2588-2606 e2586, doi:10.1016/j.neuron.2022.05.024 (2022).
35 Arsenault, J. *et al.* FMRP Expression Levels in Mouse Central Nervous System Neurons Determine Behavioral Phenotype. *Hum Gene Ther* **27**, 982-996, doi:10.1089/hum.2016.090 (2016).
36 Tinevez, J. Y. *et al.* TrackMate: An open and extensible platform for single-particle tracking. *Methods* **115**, 80-90, doi:10.1016/j.ymeth.2016.09.016 (2017).
37 Park, H. Y. *et al.* Visualization of dynamics of single endogenous mRNA labeled in live mouse. *Science* **343**, 422-424, doi:10.1126/science.1239200 (2014).
38 Yoon, Y. J. *et al.* Glutamate-induced RNA localization and translation in neurons. *Proc Natl Acad Sci U S A* **113**, E6877-E6886, doi:10.1073/pnas.1614267113 (2016).
39 Linghu, C. *et al.* Spatial Multiplexing of Fluorescent Reporters for Imaging Signaling Network Dynamics. *Cell* **183**, 1682-1698 e1624, doi:10.1016/j.cell.2020.10.035 (2020).
40 Riback, J. A. *et al.* Composition-dependent thermodynamics of intracellular phase separation. *Nature* **581**, 209-214, doi:10.1038/s41586-020-2256-2 (2020).
41 Shin, Y. *et al.* Spatiotemporal Control of Intracellular Phase Transitions Using Light-Activated optoDroplets. *Cell* **168**, 159-171 e114, doi:10.1016/j.cell.2016.11.054 (2017).
42 Park, H. *et al.* Optogenetic protein clustering through fluorescent protein tagging and extension of CRY2. *Nat Commun* **8**, 30, doi:10.1038/s41467-017-00060-2 (2017).
43 Delarue, M. *et al.* mTORC1 Controls Phase Separation and the Biophysical Properties of the Cytoplasm by Tuning Crowding. *Cell* **174**, 338-349 e320, doi:10.1016/j.cell.2018.05.042 (2018).
44 Birsa, N. *et al.* FUS-ALS mutants alter FMRP phase separation equilibrium and impair protein translation. *Sci Adv* **7**, doi:10.1126/sciadv.abf8660 (2021).
45 Goering, R. *et al.* FMRP promotes RNA localization to neuronal projections through interactions between its RGG domain and G-quadruplex RNA sequences. *Elife* **9**, doi:10.7554/eLife.52621 (2020).

46 Shu, H. *et al.* FMRP links optimal codons to mRNA stability in neurons. *Proc Natl Acad Sci U S A* **117**, 30400-30411, doi:10.1073/pnas.2009161117 (2020).
47 Kurosaki, T. *et al.* Loss of the fragile X syndrome protein FMRP results in misregulation of nonsense-mediated mRNA decay. *Nat Cell Biol* **23**, 40-48, doi:10.1038/s41556-020-00618-1 (2021).
48 Zhang, G. *et al.* Dynamic FMR1 granule phase switch instructed by m6A modification contributes to maternal RNA decay. *Nat Commun* **13**, 859, doi:10.1038/s41467-022-28547-7 (2022).

Figure 1

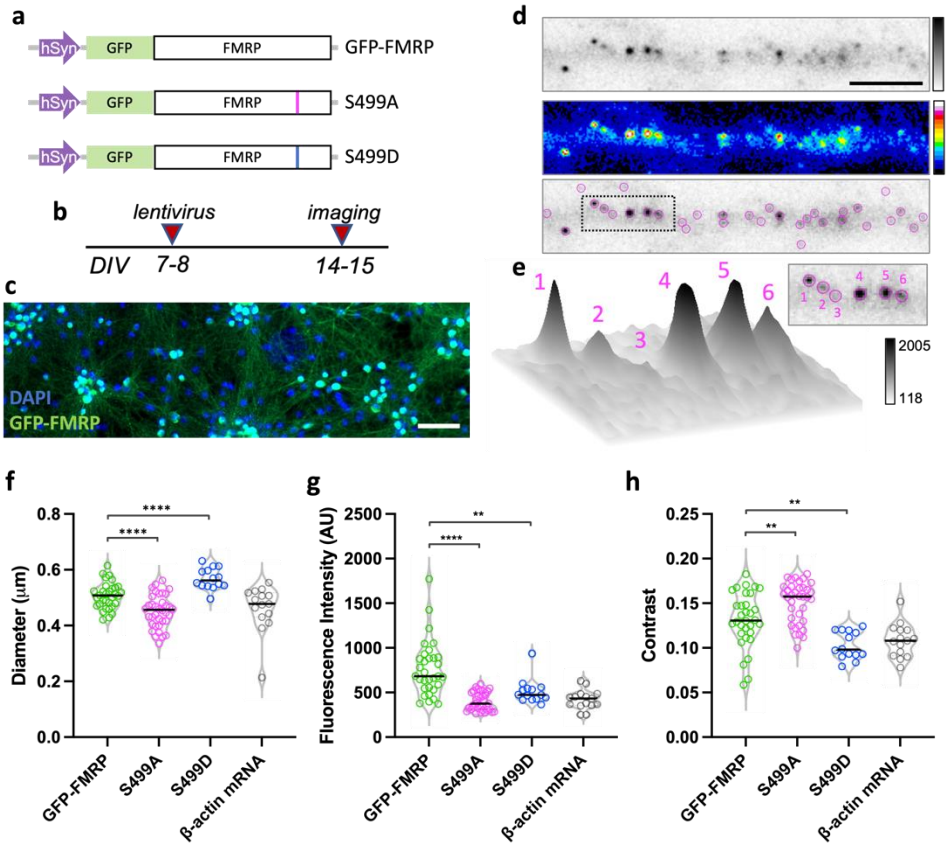
a
hSyn
GFP
FMRP
GFP-FMRP
S499A
S499D
b
lentivirus
imaging
DIV
7-8
14-15
c
DAPI
GFP-FMRP
d
e
1
2
3
4
5
6
2005
118
f
Diameter (µm)
****
GFP-FMRP
S499A
S499D
β-actin mRNA
g
Fluorescence Intensity (AU)
**
h
Contrast

Figure 2

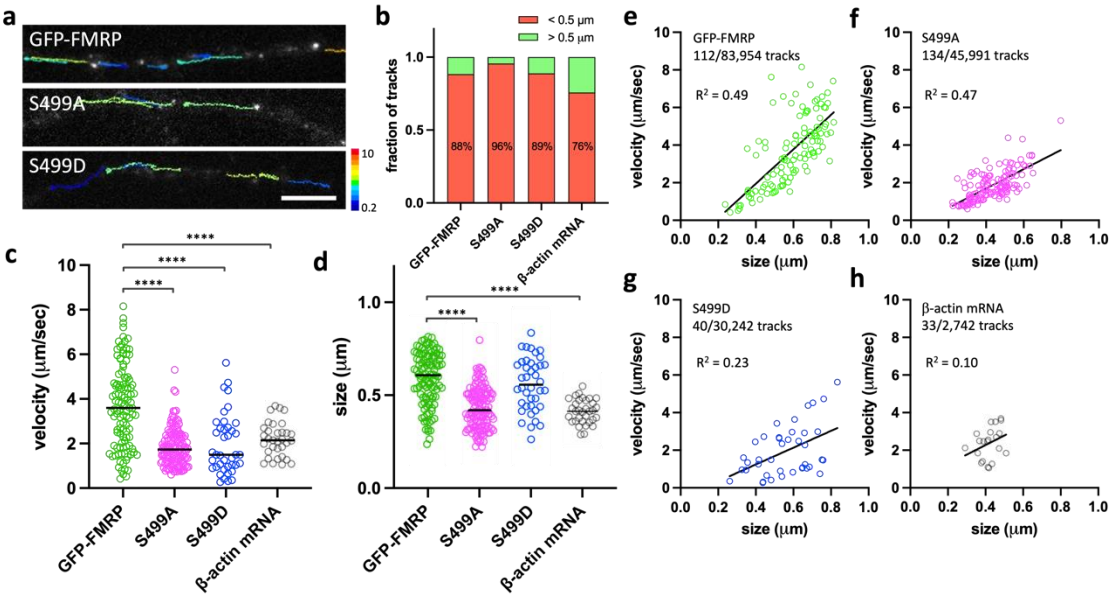
a
GFP-FMRP
S499A
S499D
10
0.2
b
< 0.5 µm
> 0.5 µm
fraction of tracks
88%
96%
89%
76%
GFP-FMRP
S499A
S499D
β-actin mRNA
c
velocity (µm/sec)
****
GFP-FMRP
S499A
S499D
β-actin mRNA
d
size (µm)
****
GFP-FMRP
S499A
S499D
β-actin mRNA
e
GFP-FMRP
112/83,954 tracks
R² = 0.49
velocity (µm/sec)
size (µm)
f
S499A
134/45,991 tracks
R² = 0.47
velocity (µm/sec)
size (µm)
g
S499D
40/30,242 tracks
R² = 0.23
velocity (µm/sec)
size (µm)
h
β-actin mRNA
33/2,742 tracks
R² = 0.10
velocity (µm/sec)
size (µm)

Figure 3

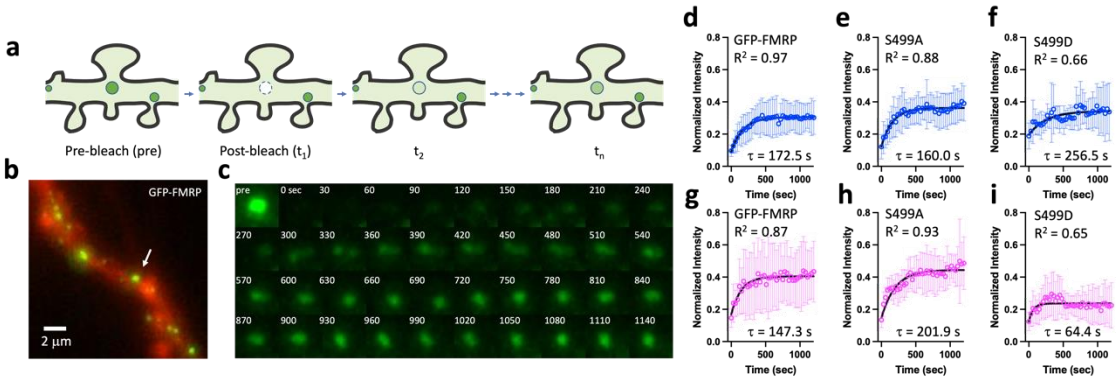
a
Pre-bleach (pre)
Post-bleach (t_1)
t_2
t_n
b
GFP-FMRP
2 µm
c
pre
0 sec
30
60
90
120
150
180
210
240
270
300
330
360
390
420
450
480
510
540
570
600
630
660
690
720
750
780
810
840
870
900
930
960
990
1020
1050
1080
1110
1140
d
GFP-FMRP
R^2 = 0.97
τ = 172.5 s
e
S499A
R^2 = 0.88
τ = 160.0 s
f
S499D
R^2 = 0.66
τ = 256.5 s
g
GFP-FMRP
R^2 = 0.87
τ = 147.3 s
h
S499A
R^2 = 0.93
τ = 201.9 s
i
S499D
R^2 = 0.65
τ = 64.4 s
Normalized Intensity
Time (sec)

Figure 4

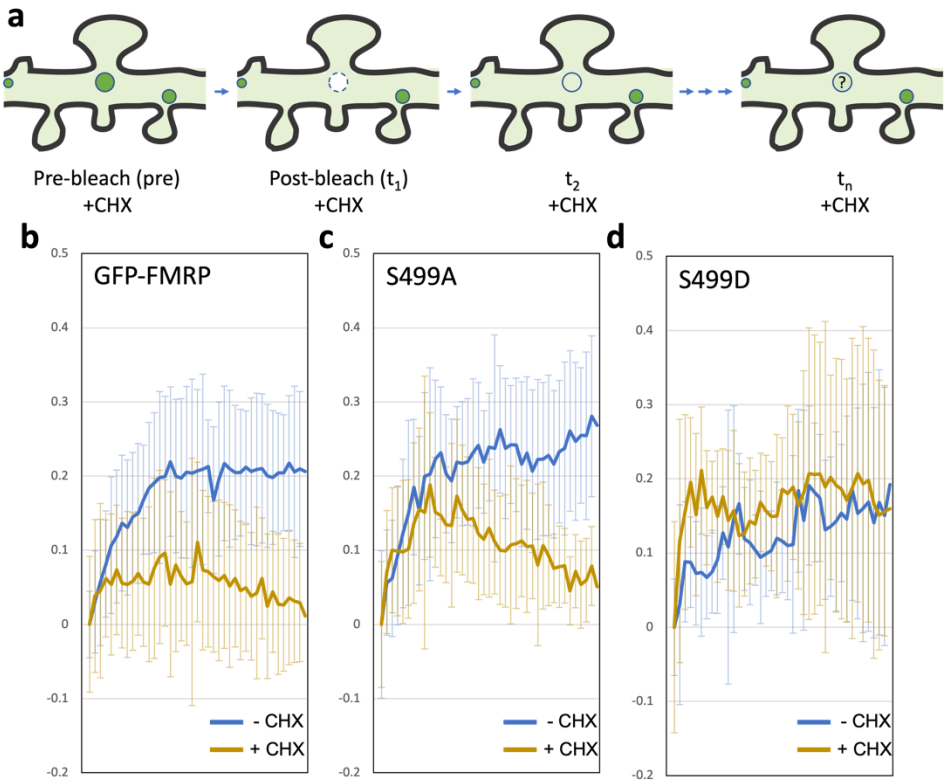
a
Pre-bleach (pre)
+CHX
Post-bleach (t_1)
+CHX
t_2
+CHX
t_n
+CHX
b
GFP-FMRP
c
S499A
d
S499D
- CHX
+ CHX
0.5
0.4
0.3
0.2
0.1
0
-0.1
-0.2

Figure S1

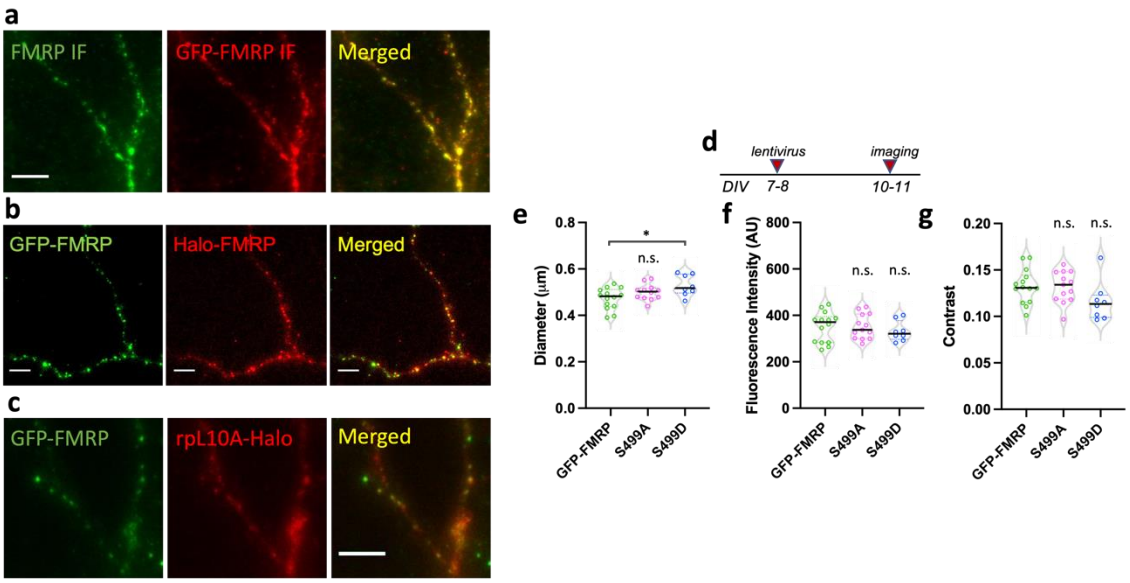
a
FMRP IF
GFP-FMRP IF
Merged
b
GFP-FMRP
Halo-FMRP
Merged
c
GFP-FMRP
rpL10A-Halo
Merged
d
lentivirus
imaging
DIV 7-8
10-11
e
Diameter (µm)
0.8
0.6
0.4
0.2
0.0
*
n.s.
GFP-FMRP
S499A
S499D
f
Fluorescence Intensity (AU)
800
600
400
200
0
n.s.
n.s.
GFP-FMRP
S499A
S499D
g
Contrast
0.20
0.15
0.10
0.05
0.00
n.s.
n.s.
GFP-FMRP
S499A
S499D

Figure S2

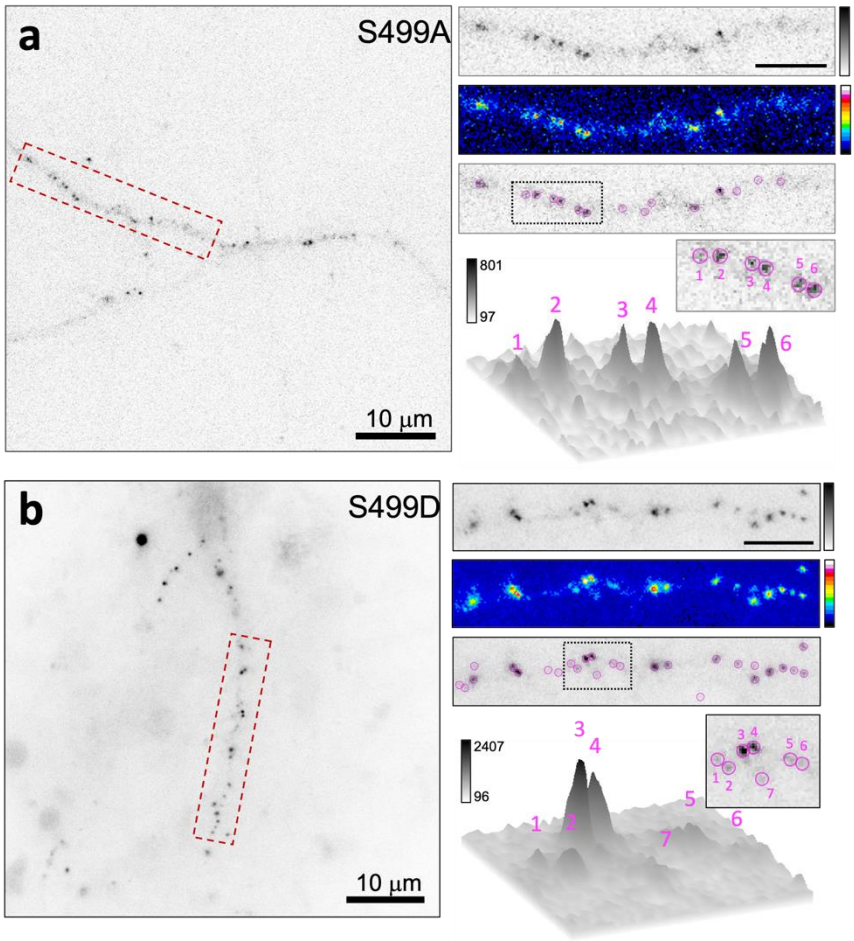

Figure S3

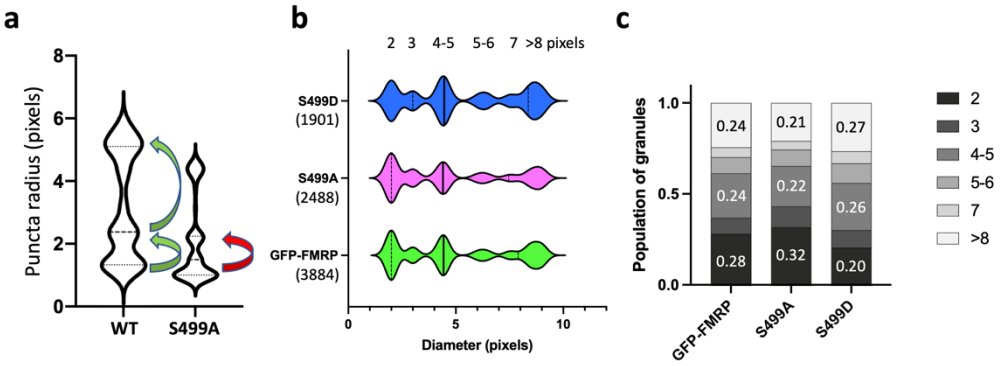
a
Puncta radius (pixels)
8
6
4
2
0
WT
S499A
b
2 3 4-5 5-6 7 >8 pixels
S499D
(1901)
S499A
(2488)
GFP-FMRP
(3884)
0
5
10
Diameter (pixels)
c
Population of granules
1.0
0.5
0.0
0.24
0.21
0.27
0.24
0.22
0.26
0.28
0.32
0.20
GFP-FMRP
S499A
S499D
2
3
4-5
5-6
7
>8

Figure S4

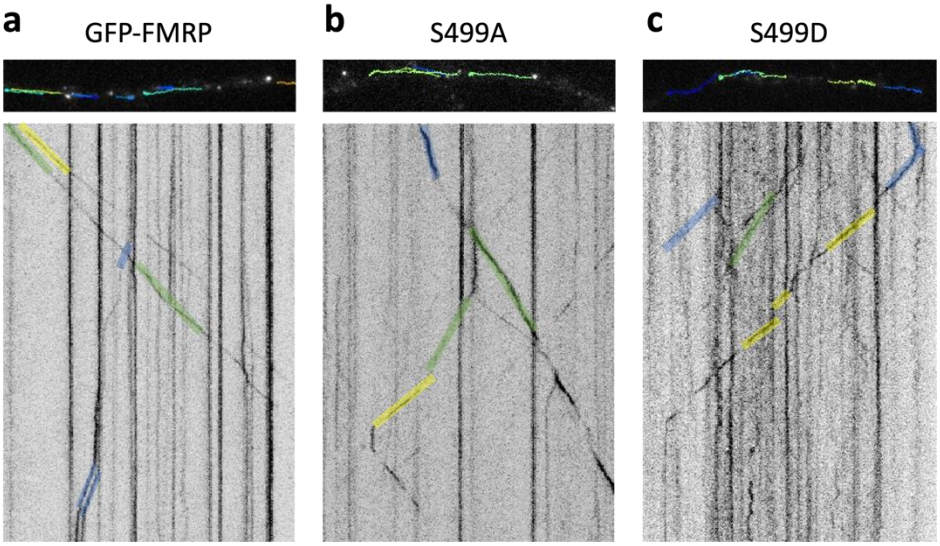

Figure S5

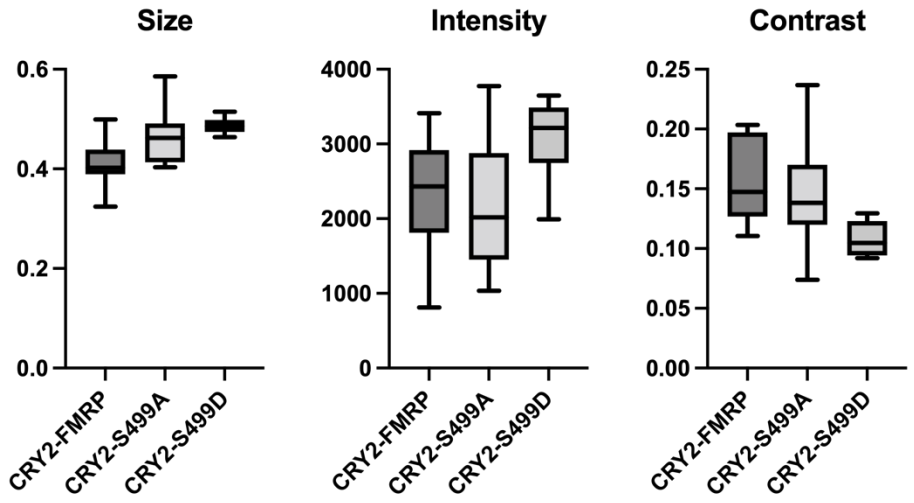
Size
0.6
0.4
0.2
0.0
CRY2-FMRP
CRY2-S499A
CRY2-S499D
Intensity
4000
3000
2000
1000
0
CRY2-FMRP
CRY2-S499A
CRY2-S499D
Contrast
0.25
0.20
0.15
0.10
0.05
0.00
CRY2-FMRP
CRY2-S499A
CRY2-S499D
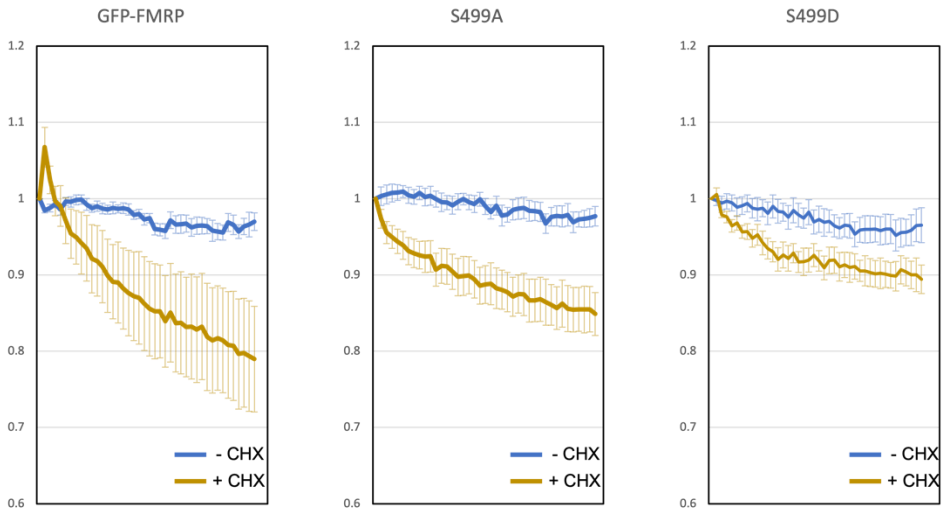
Figure S6